5-18-2007

Computational Studies of Intramolecular Hydrogen Atom Transfers in the ß-Hydroxyethylperoxy and ß -Hydroxyethoxy Radicals

Keith T. Kuwata
Macalester College

Theodore S. Dibble
State University of New York

Emily Sliz
Macalester College

Erin B. Petersen
Macalester College

Computational Studies of Intramolecular Hydrogen Atom Transfers in the β-Hydroxyethylperoxy and β-Hydroxyethoxy Radicals

Keith T. Kuwata,*,† Theodore S. Dibble,‡ Emily Sliz,† and Erin B. Petersen†

Department of Chemistry, Macalester College, Saint Paul, Minnesota 55105-1899 and Department of Chemistry, State University of New York, College of Environmental Science and Forestry, Syracuse, New York 13210

Received: January 17, 2007; In Final Form: March 27, 2007

The β-hydroxyethylperoxy (**I**) and β-hydroxyethoxy (**III**) radicals are prototypes of species that can undergo hydrogen atom transfer across their intramolecular hydrogen bonds. These reactions may play an important role in both the atmosphere and in combustion systems. We have used density functional theory and composite electronic structure methods to predict the energetics of these reactions, RRKM/master equation simulations to model the kinetics of chemically activated **I**, and variational transition state theory (TST) to predict thermal rate constants for the 1,5-hydrogen shift in **I** (Reaction 1) and the 1,4-hydrogen shift in **III** (Reaction 2). Our multi-coefficient Gaussian-3 calculations predict that Reaction 1 has a barrier of 23.59 kcal/mol, and that Reaction 2 has a barrier of 22.71 kcal/mol. These predictions agree rather well with the MPW1K and BB1K density functional theory predictions but disagree with predictions based on B3LYP energies or geometries. Our RRKM/master equation simulations suggest that almost 50% of **I** undergoes a prompt hydrogen shift reaction at pressures up to 10 Torr, but the extent to which **I** is chemically activated is uncertain. For Reaction 1 at 298 K, the variational TST rate constant is ~30% lower than the conventional TST result, and the microcanonical optimized multidimensional tunneling (μOMT) method predicts that tunneling accelerates the reaction by a factor of 3. TST calculations on Reaction 2 reveal no variational effect and a 298 K μOMT transmission coefficient of 10^5. The Eckart method overestimates transmission coefficients for both reactions.

I. Introduction

There is substantial computational evidence that intramolecular hydrogen bonds facilitate hydrogen atom transfer in β-hydroxyalkylperoxy and β-hydroxyalkoxy radicals in the atmosphere.[1−8] For example, we recently used quantum chemistry and RRKM/master equation calculations[7,8] to study intramolecular hydrogen shifts across hydrogen bonds in the second-generation alkoxy and peroxy radicals formed in the atmospheric oxidation of isoprene. There were significant uncertainties in the theoretical methods we employed. B3LYP,[9−11] MPW1K,[12] and CBS-QB3[13] predictions of hydrogen shift barriers disagreed by several kcal/mol for the peroxy radicals. Moreover, our treatment of hydrogen atom tunneling, which modeled the reaction coordinate with the asymmetric Eckart potential,[14] depended strongly on the magnitude of the transition structure's imaginary frequency. For the peroxy radicals, the B3LYP and MPW1K imaginary frequencies differed by up to 700 cm^{-1}, leading to predicted tunneling corrections that differed by as much as a factor of 10^3 at 300 K. Both uncertainties hampered our ability to predict the kinetics of these hydrogen atom transfer reactions.

The general significance of such reactions, and the importance of describing them more accurately, led us to explore small model radicals. This paper focuses on intramolecular hydrogen atom transfer in two such prototypical radicals, •$OOCH_2CH_2$-OH (**I**) and •OCH_2CH_2OH (**III**) (Reactions 1 and 2):

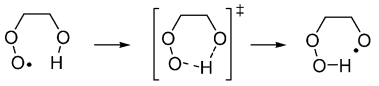

[1]

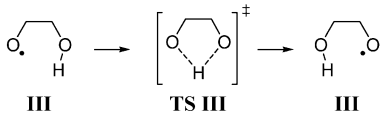

[2]

The small sizes of species **I** and **III** allow us to study the kinetics of these reactions in detail. Most fundamentally, it is computationally feasible to use highly accurate electronic structure methods to evaluate reaction barriers for **I** and **III**. These predictions can then be used to validate results obtained using density functional theory (DFT). This validation is important, given the ambiguities of our previous studies.[7,8] Using DFT, in turn, makes it feasible to tackle extensive statistical rate theory calculations, as we discuss below.

One major source of species **I** is the atmospheric oxidation of ethene. Almost 50 Tg/yr of ethene is emitted from both natural and anthropogenic sources.[15] The most important atmospheric sink for ethene is reaction with hydroxyl radical (•OH) (Reaction 3), followed by reaction with O_2 (Reaction 4):[16−18]

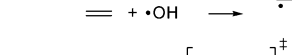

[3]

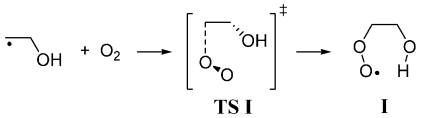

[4]

* To whom correspondence should be addressed. E-mail: kuwata@macalester.edu.
† Macalester College.
‡ State University of New York.

10.1021/jp0704113 CCC: $37.00
Published on Web 05/18/2007 PAGE EST: 10.1

These reactions lead to a chemically activated β-hydroxyethylperoxy radical (**I**) capable of prompt unimolecular reactions. Olivella and Solé,[19] using RCCSD(T)//B3LYP calculations, predicted that the lowest barrier isomerization pathway for **I** involves a 1,5-hydrogen shift to form the β-hydroperoxyethoxy radical (**II**), as shown in Reaction 1 above. Species **II** can then decompose to form •OH and two equivalents of CH_2O.

Because the predicted barrier for the 1,5-hydrogen shift in **I** (29.37 kcal/mol for Reaction 1 at 0 K) is less than the predicted amount of energy released by formation of **I** (−32.97 kcal/mol for Reaction 4 at 0 K), Olivella and Solé proposed that the dominant fate of chemically activated **I** is Reaction 1. However, other intramolecular hydrogen transfer reactions may occur:

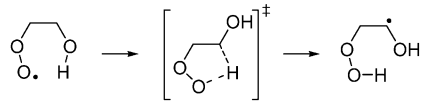

[5]

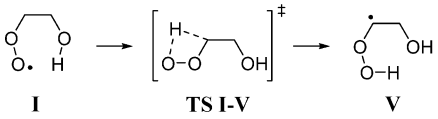

[6]

Although the 1,4-hydrogen shift (Reaction 5) and the 1,3-hydrogen shift (Reaction 6) have higher activation enthalpies, the fact that multiple conformers of **I** can undergo these higher barrier processes may enhance the contributions of Reactions 5 and 6 to the prompt chemistry of **I**.

More importantly, collisional stabilization may substantially or even completely attenuate energetically accessible unimolecular pathways. Moreover, under low [NO_x] conditions in the troposphere, once species **I** is thermalized, the 1,5-hydrogen shift (Reaction 1 above) will be negligible compared to bimolecular reactions of **I** with itself[20] or with other peroxy radicals in the troposphere.[17] It is therefore necessary to quantify the competition between thermalization and all possible prompt hydrogen shift reactions. In this paper, we present the results of RRKM/master equation simulations of the fate of chemically activated **I**. The use of a validated DFT method to generate the electronic structure inputs for these simulations allows us to model the reactivity of **I** thoroughly with only modest computational cost.

Another important context for species **I** is the combustion of ethanol, an increasingly common gasoline additive. The state of the art ethanol oxidation mechanism constructed by Marinov[21,22] predicts that a significant fraction of ethanol undergoes hydrogen atom abstraction from the methyl group (Reaction 7):

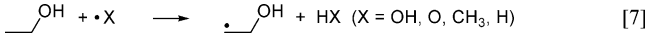

[7]

The resulting $\bullet CH_2CH_2OH$ radical then reacts with O_2 (Reaction 4 above) to form **I**. Combustion systems clearly have sufficient thermal energy to drive both the 1,5-hydrogen shift (Reaction 1 above) to form **II**, and **II**'s subsequent decomposition to 2 CH_2O + •OH. In his mechanism, Marinov includes an approximate rate coefficient expression for this process, but it would be useful to have a more accurate estimate that includes the effect of tunneling. In this paper we derive such an expression using variational transition state theory.

Under higher [NO_x] conditions in the atmosphere, collisionally stabilized **I** will be converted quantitatively via Reaction 8 to the chemically activated β-hydroxyethoxy radical (**III**):[18,23]

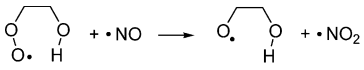

[8]

Experimental and computational studies by Vereecken, Peeters, and Orlando et al.[1,24] indicate that at 1 atm and 298 K, ~40% of **III** will undergo β-scission promptly via Reaction 9:

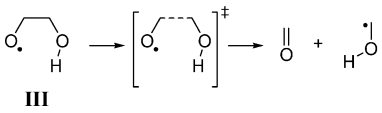

[9]

Under the same conditions, the remaining ~60% of **III** is first thermalized, and then either decomposes via Reaction 9, or reacts with O_2 (Reaction 10):[1,18,24]

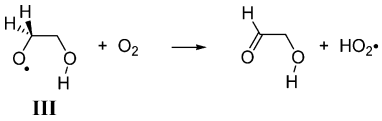

[10]

Another possible unimolecular reaction of **III** is the previously mentioned 1,4-hydrogen shift (Reaction 2):

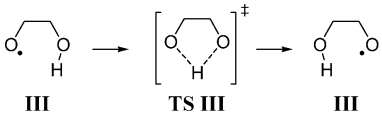

[2]

There are at least two reasons one might discount Reaction 2 in this context. The first reason is that, because it is an identity reaction, it cannot be detected experimentally without the use of isotopically labeled reagents. However, the analogous reaction in an asymmetric alkoxy radical (e.g., Reaction 11)

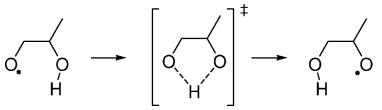

[11]

would change the fate of the radical and the product yields.

The second reason one might discount Reaction 2 is that the β-scission of **III** (Reaction 9) has a predicted barrier of ~10 kcal/mol.[1,6,24] In contrast, as we discuss below, the 1,4-hydrogen shift in **III** (Reaction 2) has a barrier of ~20 kcal/mol. Reaction 2 would therefore appear to be completely negligible under atmospheric conditions. However, tunneling can have an enormous effect on the rates on intramolecular hydrogen transfer reactions. For example, Zhang et al.[25] have predicted that the 1,2- and 1,3-hydrogen shifts in ethoxy radical have Eckart tunneling coefficients of $\sim 10^8$ at 250 K. The 1,4-hydrogen shift, as exemplified by Reaction 2, may therefore have some impact on atmospheric chemistry. In this paper, we present variational transition state theory predictions of Reaction 2's thermal rate constants, including tunneling corrections.

In our calculations of the transmission coefficients for Reactions 1 and 2, we test the predictions of the Eckart method against more rigorous multidimensional methods. It is known that for bimolecular reactions, the arbitrary shape of the Eckart potential can sometimes lead to unreliable estimates of tunneling probabilities,[26,27] and that the Eckart model's one-dimensional treatment of tunneling neglects the deviations from the minimum energy path that occur when a hydrogen atom moves between two heavy atoms.[28] However, there has been little testing of the Eckart method for unimolecular reactions.[25,29] The greatest computational challenge of multidimensional tunneling methods

TABLE 1: Relative Energies (0 K, kcal/mol) for the Conformers in Figure 1

conformer	B3LYP[a]	B3LYP[b]	MPW1K[b]	BB1K[b]	CCSD(T)[c]	CBS-QB3[d]
a	0.00	0.00	0.00	0.00	0.00	0.00
b	1.13	0.21	−0.05	0.15	0.45	0.05
c	1.79	0.42	0.11	0.43	1.34	0.51
d	2.69	1.31	1.14	1.35	2.00	0.96
e	3.44	1.64	1.52	1.85	2.99	1.56
f	3.03	1.75	1.42	1.69	2.19	1.65
g	2.77	1.88	1.72	1.98	2.22	1.87
h	3.22	2.28	2.12	2.34	2.73	2.01
i	3.05	2.17	1.99	2.27	2.48	2.18
j	3.74	2.36	2.26	2.57	3.43	2.24
k	3.94	2.27	1.92	2.34	3.27	2.37
l	3.98	2.66	2.42	2.83	3.54	2.78
m	3.99	—[e]	—[e]	—[e]	3.52	—[e]
MAD[f]	1.15	0.12	0.19	0.15	0.71	0.00

[a] With the 6-31G(d,p) basis set; taken from Vereecken and Peeters.[1] [b] With the 6-31+G(d,p) basis set. [c] CCSD(T)/6-31G(d,p)//B3LYP/6-31G(d,p); taken from Vereecken and Peeters.[1] [d] Based on B3LYP/6-311G(2d,d,p) optimized geometries. [e] Not a minimum for this model chemistry. [f] MAD = mean absolute deviation from the CBS-QB3 relative energies. Conformer **m** not included.

TABLE 2: Relative Energies (0 K, kcal/mol) for the Conformers in Figure 2

conformer	B3LYP[a]	B3LYP[b]	MPW1K[b]	BB1K[b]	CCSD(T)[c]	CBS-QB3[d]
a	0.00	0.00	0.00	0.00	0.00	0.00
b	1.86	1.05	0.98	1.31	1.58	1.15
c	2.70	1.89	1.80	—[e]	2.25	1.70
d	2.21	1.69	1.64	1.83	2.07	1.78
e	3.34	2.90	2.86	3.27	3.15	2.67
MAD[f]	0.56	0.12	0.12	0.20[g]	0.35	0.00

[a] With the 6-31G(d,p) basis set; taken from Vereecken and Peeters.[1] [b] With the 6-31+G(d,p) basis set. [c] CCSD(T)/6-31G(d,p)//B3LYP/6-31G(d,p); taken from Vereecken and Peeters.[1] [d] Based on B3LYP/6-311G(2d,d,p) optimized geometries. [e] Not a minimum for this model chemistry. [f] MAD = mean absolute deviation from the CBS-QB3 relative energies. [g] This MAD does not include conformer **c**.

is the need for repeated computation of Hessians along the minimum energy path. Our use of a validated DFT method makes such calculations both reliable and feasible.

II. Computational Methods

II.A. Electronic Structure Calculations. Three hybrid DFT methods, B3LYP, MPW1K, and BB1K, were used to predict the electronic energies, optimized geometries, and harmonic vibrational frequencies of the single conformers of **TS I−II** and **TS III**, and all conformers of species **I**, **II**, and **III**, in Reactions 1 and 2 above. Each reported minimum had all real frequencies, and each reported transition structure had one imaginary frequency. We determined the minima associated with each transition structure by animation of the imaginary frequency and, in some cases, with IRC calculations. To determine the zero-point energy corrections to the electronic energies, the harmonic vibrational frequencies were scaled as recommended by Radom[30] and Truhlar.[31,32] All calculations on radicals employed unrestricted wave functions.

B3LYP[9−11] is one of the more commonly used functionals, but it often underestimates barriers to H-atom transfer reactions in open-shell systems.[12,31,33−35] MPW1K[12] and BB1K[32] are Truhlar and co-workers' re-parametrizations of the mPW1PW91[36,37] and B1B95[38,39] hybrid DFT methods, respectively. In both methods, the fraction of Hartree−Fock exchange is optimized to reproduce accurately known barrier heights for intermolecular hydrogen transfer reactions. BB1K is comparable to MPW1K in the ability to predict the energies and geometries of transition states and is superior to MPW1K in the ability to predict thermochemical properties like atomization energies.[32] With all DFT methods, the 6-31+G(d,p)[40−42] basis set was used for all conformers, and the MG3S[43,44] (that is, 6-311+G(2df,2p)) basis set was used for the most stable conformers.

The G3S, CBS-QB3, G3//B3LYP, G3SX, and multi-coefficient Gaussian-3 (MCG3) composite methods were also used to predict the energies of **TS I−II**, **TS III**, and the most stable conformers of **I**, **II**, and **III**. Each of these methods uses a series of single point calculations to approximate a single point calculation at the QCISD(T) or CCSD(T) level of theory with a large (or infinite) basis set. The G3S method[45] is based on an MP2(full)/6-31G(d) optimized geometry, whereas the CBS-QB3,[13] G3//B3LYP,[46] and G3SX[47] methods are all based on geometries optimized with B3LYP and either a double-ζ or triple-ζ basis set.

Although the G3S, CBS-QB3, G3//B3LYP, and G3SX model chemistries were originally parametrized to reproduce thermochemical properties, each has received at least some validation of its ability to predict accurate hydrogen shift barriers.[33,48−50] Nevertheless, one may take issue with the quality of the MP2 and B3LYP transition state geometries these methods employ. Truhlar and co-workers have provided evidence[51,52] that for open-shell systems, the higher levels of electron correlation provided by the QCISD, CCSD, and multi-coefficient QCISD[53] (MC-QCISD) methods provide far more accurate transition state geometries. Accordingly, we attempted optimizations of all of the species of interest using each of these methods. All optimizations of the minima **I**, **II**, and **III** succeeded. However, all of the QCISD searches for transition structure **TS III** converged to unphysical structures in which the two partial O−H bonds were not of equal length. All QCISD searches for **TS I−II**, and all MC-QCISD searches for both **TS I−II** and **TS III**, failed to converge. However, the CCSD/6-31G(d) geometry optimization of **TS III** did converge. This geometry, and the CCSD/6-31G(d) geometry of **III**, were used as the basis for MCG3 calculations employing Lynch and Truhlar's version 3m parameters.[54] Also, given the evidence[32] that the BB1K functional can predict transition state geometries as accurately as QCISD, MCG3 calculations were also performed based on the BB1K/MG3S optimized geometries of **III** and **TS III**. All treatments of electron correlation, except for the MP2(full)/6-31G(d) optimizations, neglected the contribution of core electrons.

Most of the quantum chemistry calculations were carried out using the Gaussian 03 program suite.[55] CCSD optimizations were performed using ACES2,[56] and MC-QCISD and MCG3 calculations were performed using MULTILEVEL.[57]

II.B. RRKM/Master Equation Calculations. We used Barker's MultiWell program suite[58,59] to solve the master equation for the formation (Reaction 4 above) and isomerization (Reactions 1, 5, and 6 above) of the β-hydroxyethylperoxy radical (**I**). The zero-point corrected relative energies of all possible conformers of all participating species were taken from our BB1K/6-31+G(d,p) calculations. Microcanonical rate constants $k(E)$ were computed using RRKM theory,[60] with the required sums and densities of states being calculated based on BB1K/6-31+G(d,p) optimized geometries and harmonic frequencies scaled by 0.9561.[32] We did not treat low-frequency internal rotations as hindered rotors.

We treated collisional stabilization with the exponential-down model, using an energy grain size of 10 cm^{-1} and assuming an average energy transferred per collision ($\langle E_d \rangle$) of 300 cm^{-1}.[61] The bath gas was N_2 at 298 K, with Lennard-Jones parameters

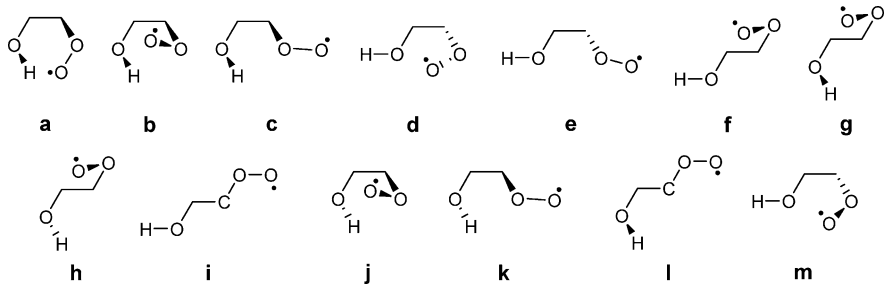

Figure 1. All stable conformers of the β-hydroxyethylperoxy radical (species **I**).

of $\sigma = 3.74$ Å and $\epsilon = 82$ K.[62,63] Following the same procedures[64−67] used in our study of isoprene ozonolysis,[68] we estimated Lennard-Jones parameters of $\sigma = 4.31$ Å and $\epsilon = 297$ K for the $\bullet C_2H_5O_3$ minima and transition structures.

Each simulation was run for 10^3 collisions to ensure that the pseudo steady state[69] was achieved. Trials were run at pressures of 1, 10, 50, 100, 200, 300, 400, 500, 600, 700, and 760 Torr. Each pseudo steady-state yield reported is the average result of 10^4 Monte Carlo simulations. For a yield of ~1, the statistical uncertainty is no higher than ±0.009. For a yield of ~0.001, the statistical uncertainty is ±0.0005. Details of how the initial energy distribution of **I** was represented in a given simulation are given in the Results and Discussion section below.

II.C. Transition State Theory Calculations. All of the rate constants reported here were calculated using Truhlar's POLYRATE 9.1[70] and GAUSSRATE 9.1.[71] All energies, gradients, and Hessians were computed with the BB1K/6-31+G(d,p) method, with all vibrational modes treated under the harmonic approximation.

We computed thermal rate constants for Reactions 1 and 2 above using both canonical variational transition state theory (CVT)[72−74] and improved canonical variational theory (ICVT),[75,76] which removes contributions to the rate constant at energies below that of the saddle point. For both reactions the CVT and ICVT results agree at all temperatures to three significant figures. We also report rate constants computed with conventional, non-variational transition state theory (TST).

CVT calculations on Reaction 1 revealed two local maxima in the ground-state vibrationally adiabatic potential curve ($V_a^G(s)$) and the free energy of activation curves ($\Delta G^{GT,0}(T,s)$) on either side of the saddle point. This can give rise to significant recrossing effects which cause the CVT method to overestimate the classical rate constant. We corrected for these effects by using the canonical unified statistical (CUS)[77] method.

We treated hydrogen atom tunneling multidimensionally[78] in Reactions 1 and 2 with the small-curvature tunneling (SCT),[79] version-4 large-curvature tunneling (LCT),[80] and microcanonical optimized multidimensional tunneling (μOMT)[81] approximations. Convergence of the transmission coefficients, $\Gamma(T)$, to three significant figures required computation of the minimum energy path from $s = -2.2$ a_o to $s = +2.2$ a_o, with a step size of 0.00025 a_o and Hessians being computed every five steps.

Finally, we also estimated the impact of tunneling on thermal rate constants using the asymmetric Eckart potential.[14,82] Eckart transmission coefficients depend only on the reaction barrier, reaction energy, and the magnitude of the imaginary frequency, ν^*, of the vibration along the reaction coordinate, and are particularly sensitive to the value of ν^*. We computed Eckart $\Gamma(T)$ values with Truong's VKLab 1.0,[83] again based on BB1K/6-31+G(d,p) electronic structure data.

III. Results and Discussion

III.A. Conformational Analysis of the Alkoxy and Alkylperoxy Radicals. Figures 1 and 2 show all possible conformers

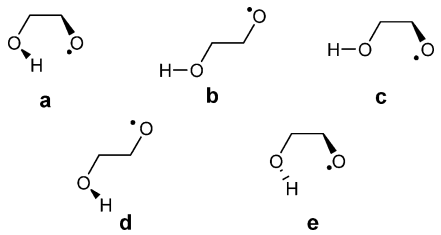

Figure 2. All stable conformers of the β-hydroxyethoxy radical (species **III**).

for species **I** and **III** identified by Vereecken and Peeters'[1] and our DFT, CCSD(T), and CBS-QB3 calculations. Tables 1 and 2 present the zero-point corrected relative energies of each of the species in the schemes. We will assume that the CBS-QB3 relative energies are the most accurate and judge the accuracy of the each of the other methods by the mean absolute deviation (MAD) of that method's relative energies from the CBS-QB3 predictions.

For species **I** (Table 1), all methods except for MPW1K agreed that conformer **a** (Figure 1), which possesses an intramolecular hydrogen bond between the OH group and the terminal peroxy oxygen, is the most stable. The calculations with the 6-31+G(d,p) basis set had MADs of less than 0.20 kcal/mol; the calculations with the 6-31G(d,p) basis set were significantly less accurate. This is consistent with Truhlar's recommendation[12,43] that diffuse functions always be placed on non-hydrogen atoms in DFT calculations. Given that only the B3LYP/6-31G(d,p) method predicted that conformer **m** corresponds to a minimum on the potential energy surface, its predicted existence may be merely an artifact of using a small basis set. It is also noteworthy that all three DFT methods, when used with the 6-31+G(d,p) basis set, were more accurate than the single point CCSD(T)/6-31G(d,p) method. However, as Vereecken and Peeters themselves note,[1] the 6-31G(d,p) basis set is rather small for as high as level of theory as CCSD(T).

For species **III** (Table 2), all methods predict that conformer **a** (Figure 2), which possesses an intramolecular hydrogen bond, is the most stable structure. Again, the DFT calculations with the 6-31+G(d,p) basis set agree better with the CBS-QB3 predictions than either B3LYP or CCSD(T) calculations with the 6-31G(d,p) basis set. The BB1K/6-31+G(d,p) method predicts that conformer **c** is a transition structure, not a minimum. However, based on CBS-QB3 free energies, conformers **a** and **b** should account for almost 90% of the equilibrium population of species **III** at 298 K. Therefore, even if conformer **c** actually exists, its neglect would introduce only a minor error.

III.B. Quantum Chemistry of the Hydrogen Shift Reactions. The Supporting Information contains a detailed discussion of the geometries predicted for the species in Reactions 1 and 2. Here we focus on the energetics. Table 3 shows the barriers

TABLE 3: Predicted Energetics (0 K, kcal/mol) for Reaction 1

method	barrier	reaction energy
B3LYP/6-31G(d,p)	18.34	18.87
B3LYP/6-31+G(d,p)	18.97	19.11
B3LYP/MG3S	19.10	19.27
MPW1K/6-31+G(d,p)	24.79	19.51
MPW1K/MG3S	24.70	20.00
BB1K/6-31+G(d,p)	24.03	20.36
BB1K/MG3S	23.79	20.82
CBS-QB3	23.60	20.51
G3S	24.73	22.33
G3//B3LYP	26.95	21.39
G3SX	25.00	21.62
MCG3[a]	23.59	21.79
RCCSD(T)/6-311+G(3df,2p)[b]	29.37	20.77

[a] Based on BB1K/MG3S optimized geometries and vibrational frequencies. [b] Taken from Olivella and Solé;[19] based on B3LYP/6-31G(d,p) optimized geometries and vibrational frequencies.

TABLE 4: Predicted Barriers (0 K, kcal/mol) for Reaction 2

method	barrier
B3LYP/6-31G(d,p)	12.42
B3LYP/6-31+G(d,p)	13.15
B3LYP/MG3S	13.69
MPW1K/6-31+G(d,p)	23.51
MPW1K/MG3S	23.44
BB1K/6-31+G(d,p)	21.15
BB1K/MG3S	20.98
CBS-QB3	18.45
G3S	25.77
G3//B3LYP	21.21
G3SX	20.12
MCG3[a]	22.67
MCG3[b]	22.75

[a] Based on the BB1K/MG3S optimized geometries and vibrational frequencies. [b] Based on the CCSD/6-31G(d) optimized geometries and vibrational frequencies.

and energies of reaction predicted for Reaction 1, and Table 4 shows the barriers predicted for Reaction 2.

The predicted barriers for Reaction 1 vary widely, from 18−29 kcal/mol, whereas the predicted reaction energies vary less, from 19−22 kcal/mol. For all DFT methods, increasing the basis set size from 6-31+G(d,p) to MG3S has very little impact on the predicted barrier. Although none of the model chemistries in Table 3 is an absolutely authoritative method of predicting hydrogen shift barriers, Lynch and Truhlar's benchmarking[54] suggests that the MCG3//BB1K/MG3S prediction should be the most accurate. All the B3LYP barriers are 4−5 kcal/mol lower than the MCG3 barrier. This is consistent with previous studies[12,31,33−35] and occurs in spite of the fact that the B3LYP transition structures, as discussed in the Supporting Information, are later than those predicted by other methods. Indeed, Olivella and Solé's[19] very high level single point RCCSD(T) barrier, based on B3LYP/6-31G(d,p) geometries, and the composite G3//B3LYP barrier, based on B3LYP/6-31G(d) geometries, are 3−6 kcal/mol higher than the MCG3 barrier. This is consistent with the use of a later transition structure. However, the other composite methods based on B3LYP geometries, CBS-QB3 and G3SX, agree to within 1 kcal/mol of the MCG3 barrier. The other methods used, G3S (based on MP2 geometries), MPW1K, and BB1K, likewise all agree with MCG3 to within 1 kcal/mol. The fact that a number of very different methods all predict a barrier of 24−25 kcal/mol provides strong evidence that the RCCSD(T) barrier is too high.

For Reaction 2 (Table 4), the predicted barriers also vary widely, from 12−26 kcal/mol. Again, for all DFT methods, increasing the basis set size from 6-31+G(d,p) to MG3S has very little impact on the predicted barrier. As with Reaction 1, we will assume here that the MCG3 predictions are the most accurate. The MCG3 barriers computed with the BB1K/MG3S and CCSD/6-31G(d) geometries, which agree to within 0.1 kcal/mol, have an average value of 22.71 kcal/mol. (The agreement is not surprising, given the similarities in the geometries, as reported in Table 2S in the Supporting Information.) The B3LYP barriers are 9−10 kcal/mol lower than the average MCG3 barrier, again consistent with previous studies. Likewise, the composite methods based on B3LYP geometries, CBS-QB3, G3//B3LYP, and G3SX, are 2−4 kcal/mol lower than MCG3. On the other hand, G3S, based on MP2 geometries, is 3 kcal/mol higher than MCG3. Finally, compared to the results for Reaction 1, the MPW1K and BB1K barriers for Reaction 2 do not agree as well with each other or with the MCG3 barriers. Nevertheless, the predictions deviate from the MCG3 values by less than 2 kcal/mol.

Overall, given the ability of BB1K to reproduce the results of more rigorous methods for minima (Tables 1 and 2) and barrier heights (Tables 3 and 4), and its previous validation for transition structure geometries,[32] we decided to rely on BB1K to predict electronic structure data for our master equation (Section C) and transition state theory (Sections D and E) calculations. (Although MPW1K performed as well as BB1K for the molecules in this study, we have previously found problems with MPW1K's treatment of oxo-substituted peroxy radicals.[84]) Because increasing the basis set size from 6-31+G(d,p) to MG3S had little effect on the above predictions, we also decided to use the smaller basis set for all subsequent calculations.

III.C. Master Equation Simulations of the β-Hydroxyethylperoxy Radical. We considered the following possible reactions in our simulations:

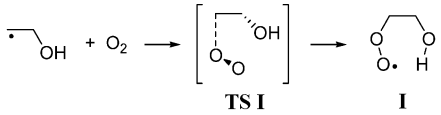

[4]

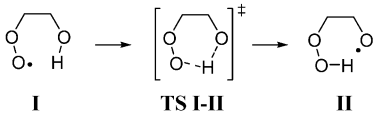

[1]

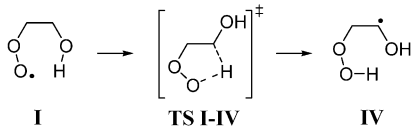

[5]

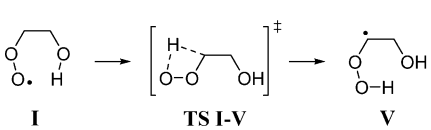

[6]

Reaction 4, the formation of the most stable conformer of β-hydroxyethylperoxy radical (species **Ia**, Figure 1), was the entrance channel. The initial energy of **Ia** was represented by a shifted thermal distribution[60] truncated at the zero-point corrected energy of transition structure **TS I**. A three-dimensional rendering of **TS I**, which has not reported in previous studies of this system, and the other species in Reaction 4 is shown in Figure 3. (Although the addition of O_2 to alkyl radicals is typically barrierless, the existence of this first-order saddle point was confirmed with both B3LYP/6-31+G(d,p) and MPW1K/

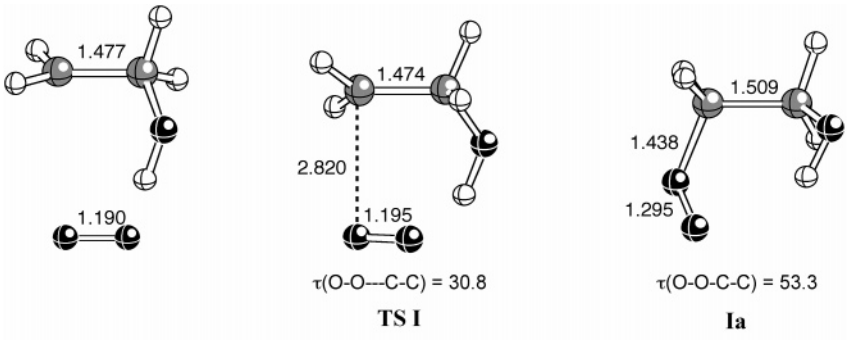

Figure 3. Optimized geometries for the species in Reaction 4. Note that gray represents carbon, black represents oxygen, and white represents hydrogen. Bond lengths (in Å) and dihedral angles (in degrees) obtained at the BB1K/6-31+G(d,p) level.

TABLE 5: Relative Energies (0 K; kcal/mol) for the Species in the Trial A Simulations[a]

species	energy
I	0.00 − 2.83[b]
TS I	36.86
TS I−II	24.03
TS I−IV	31.48−33.76[b]
TS I−V	45.46−48.46[b]

[a] From BB1K/6-31+G(d,p) calculations. [b] Range of energies indicates the existence of more than one conformer.

TABLE 6: Master Equation Yields for Trial A

Torr	species **I**	•$C_2H_4OH + O_2$	species **II**	species **IV**	species **V**
1	0.029	0.030	0.927	0.014	0.000
10	0.498	0.015	0.480	0.007	0.000
50	0.841	0.006	0.152	0.003	0.000
100	0.913	0.003	0.083	0.001	0.000
200	0.955	0.002	0.043	0.001	0.000
300	0.969	0.001	0.031	0.000	0.000
400	0.978	0.001	0.020	0.000	0.000
500	0.980	0.001	0.019	0.000	0.000
600	0.985	0.000	0.014	0.000	0.000
700	0.987	0.000	0.013	0.000	0.000
760	0.987	0.000	0.013	0.000	0.000

6-31+G(d,p) calculations.) In both **TS I** and **I**, the O−O bond is synclinal to the C−C bond. Geometrically, **TS I** is quite early, with an extremely long partially formed C−O bond of 2.820 Å, and an O−O bond only 0.005 Å longer than in the O_2 reactant.

Reactions 1, 5, 6, and the reverse of Reaction 4 were the exit channels. Reactions 1, 5, and 6 were treated as irreversible because the radicals formed in these reactions should either decompose more rapidly or (for **IV** and **V**) react with O_2 more rapidly than they can back-react. Figures 1S and 2S in the Supporting Information present the relative energies for all possible conformations of the reactants and transition structures of these exit channels. These include the four conformers of **TS I−IV** (Figure 1S) and the seven conformers of **TS I−V** (Figure 2S). Our mechanism also explicitly included the 25 transition structures interconnecting the 12 valid conformers (Table 1) of the β-hydroxyethylperoxy radical. Table 5 summarizes the zero-point corrected BB1K/6-31+G(d,p) relative energies for the wells and the exit channel barriers.

Table 6 presents the average pseudo steady-state yields as a function of pressure for each of the possible outcomes of the simulations (which we will label Trial A) based on the energies in Table 5: collisional stabilization of species **I** (in any of the 12 possible conformations), reversion to the •C_2H_4OH and O_2 reactants, formation of **II** via the 1,5-hydrogen shift, formation of **IV** via the 1,4-hydrogen shift, and formation of **V** via the 1,3-hydrogen shift.

TABLE 7: Master Equation Yields for Trial B

Torr	species **I**	•$C_2H_4OH + O_2$	species **II**	species **IV**	species **V**
1	0.448	0.082	0.469	0.001	0.000
10	0.881	0.027	0.093	0.000	0.000
50	0.966	0.009	0.026	0.000	0.000
100	0.983	0.004	0.013	0.000	0.000
200	0.991	0.002	0.006	0.000	0.000
300	0.994	0.002	0.005	0.000	0.000
400	0.995	0.001	0.003	0.000	0.000
500	0.998	0.000	0.002	0.000	0.000
600	0.998	0.001	0.002	0.000	0.000
700	0.997	0.001	0.002	0.000	0.000
760	0.998	0.001	0.001	0.000	0.000

For pressures of ∼10 Torr or lower, a majority of the peroxy radicals react. The dominant reaction is the 1,5-hydrogen shift, with non-negligible contributions from the 1,4-hydrogen shift and decomposition to •C_2H_4OH and O_2. Moreover, all four conformers of **TS I−IV** contributed to the overall yield of **IV** (results not shown). This reflects the importance of treating all conformers in kinetics simulations, as noted by Vereecken and Peeters.[85]

At higher pressures, thermalization of the peroxy radical dominates; at 1 atm only ∼1% of the radicals are predicted to undergo the 1,5-hydrogen shift. As discussed above, bimolecular reactions will be far more rapid than isomerization for thermalized **I**. Moreover, given that species **II** is only ∼4 kcal/mol more stable than **TS I−II** (Table 3), it is likely that formation of **II** is partially reversible. Hence, the formation of **II**, and its subsequent decomposition to •OH and two equivalents of CH_2O,[19] will be important to atmospheric chemistry only at low pressures.

Another issue with Trial A is the extent to which species **I** is chemically activated. BB1K/6-31+G(d,p) predicts that the O_2 addition transition structure (**TS I**) is 5.12 kcal/mol higher in energy than the separated •C_2H_4OH and O_2 reactants. This barrier is probably too high, given that the geometries of the •C_2H_4OH and O_2 moieties in **TS I** are only slightly distorted from those of the separated •C_2H_4OH and O_2 reactants (Figure 3). To quantify the effect of entrance channel energy, we performed a set of simulations (labeled Trial B) with the energy of **TS I** lowered to 31.74 kcal/mol, which corresponds to the total BB1K/6-31G(d,p) energy of •$C_2H_4OH + O_2$ relative to conformer **Ia**. All other energies were the same as in Table 5. The results are presented in Table 7.

As expected, decreasing the amount of chemical activation in the peroxy radical decreases the amount of prompt chemistry. In Trial B, a majority of peroxy radicals undergo the 1,5-hydrogen shift only at pressures of less than 1 Torr. As in Trial A, no formation of **V** via the 1,3-hydrogen shift was observed.

Finally, we calculated master equation yields based on the RCCSD(T)/6-311+G(3df,2p) single-point energies, as sum-

TABLE 8: Relative Energies (0 K; kcal/mol) for the Species in the Trial C Simulations[a]

species	energy
I	0.00
TS I	32.97
TS I−II	29.37
TS I−IV	32.11
TS I−VI	35.13

[a] From the RCCSD(T)/6-311+G(3df,2p)//B3LYP/6-31G(d,p) calculations of Olivella and Solé.[19]

TABLE 9: Master Equation Yields for Trial C

Torr	species **I**	$\bullet C_2H_4OH + O_2$	species **II**	species **IV**	species **VI**
1	0.770	0.185	0.044	0.001	0.000
10	0.935	0.057	0.009	0.000	0.000
50	0.980	0.018	0.002	0.000	0.000
100	0.987	0.011	0.001	0.000	0.000
200	0.994	0.005	0.000	0.000	0.000
300	0.995	0.004	0.000	0.000	0.000
400	0.998	0.003	0.000	0.000	0.000
500	0.998	0.002	0.000	0.000	0.000
600	0.999	0.001	0.000	0.000	0.000
700	0.999	0.000	0.000	0.000	0.000
760	0.999	0.000	0.000	0.000	0.000

marized in Table 8, from Olivella and Solé's[19] study. In this set of simulations (labeled Trial C) we replicated Olivella and Solé's mechanism by including only the most stable conformer of **TS I−IV**, neglecting any putative contribution from the 1,3-hydrogen shift, and including a reaction involving the concerted loss of HOO• from the peroxy radical (Reaction 12):

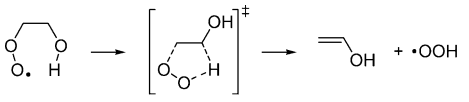

I **TS I-VI** **VI** [12]

Unlike Olivella and Solé, we assumed the existence of a first-order saddle point (**TS I**) between $\bullet C_2H_4OH + O_2$ and **I**, but, as in Trial B, we set the energy of **TS I** to that of the separated $\bullet C_2H_4OH + O_2$ reactants. The results are presented in Table 9.

Based on the RCCSD(T) energies, less than 25% of the peroxy radicals undergo prompt reaction even at 1 Torr, and the 1,4-hydrogen shift and the loss of HOO• are negligible at all pressures studied. The low yields of species **II** even at very low pressures is consistent with the high barrier of 29.37 kcal/mol predicted for the 1,5-hydrogen shift (Table 8). However, as discussed in Section B, it is likely that the RCCSD(T) barrier is too high. Therefore, the actual extent to which the β-hydroxyethylperoxy radical undergoes prompt chemistry is probably bracketed by the results of Trial A (Table 6) and Trial B (Table 7). That is, the prompt formation of **II** (and its subsequent decomposition to form 2 $CH_2O + \bullet OH$) should be a minor, but non-negligible, process at higher altitudes in the troposphere.

III.D. Transition State Theory Calculations on the 1,5-Hydrogen Shift in the β-Hydroxyethylperoxy Radical. Table 10 presents the TST, CVT, and CUS thermal rate constants predicted for Reaction 1:

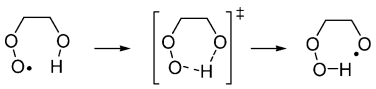

I **TS I-II** **II** [1]

To simplify the calculation, only the most stable conformers of **I** and **II** were considered. Table 10 also indicates the location of the canonical variational transition state, s_*^{CVT}, as well as the transmission coefficients Γ predicted with the SCT, LCT, μOMT, and Eckart methods.

The first thing to note is a significant variational effect on the predicted rate constant, especially at lower temperatures. At 200 K, the CVT rate constant is a factor of 2 smaller than the TST rate constant. At 298 K, the CVT rate constant is only ~30% lower, and at higher temperatures, the CVT and TST rate constants are nearly the same. Temperature also has a large effect on the location of the transition state. At 200 K, the variational transition state lies $0.22a_o$ past the saddle point, whereas at higher temperatures the variational transition state switches to the reactant side of the saddle point. This reflects, as mentioned in Section IIC, the existence of two maxima in the $V_a^G(s)$ and $\Delta G^{GT,0}(T,s)$ curves. The relative heights of these two maxima evolve as a function of temperature. More precise calculations (not tabulated) indicate that up to 549 K, the higher peak in the $\Delta G^{GT,0}(T,s)$ curve lies on the product side ($s_*^{CVT}(549\ \mathrm{K}) = 0.175$). At 550 K and higher, the higher peak in the $\Delta G^{GT,0}(T,s)$ curve lies on the reactant side ($s_*^{CVT}(550\ \mathrm{K}) = -0.008$). Analogous behavior has been predicted for the $Cl + CH_4 \rightarrow HCl + CH_3$ reaction.[86,87] The existence of two dynamical bottlenecks leads to more recrossing at the transition state, and therefore smaller rate constants than predicted by the CVT method. However, the impact is small; the CUS rate constants are only 0.6% to 1% lower than the CVT rate constants.

All methods predict that, as expected, tunneling has a smaller effect as the temperature increases. Of the semiclassical tunneling methods available in POLYRATE, μOMT agrees best with fully quantal calculations,[88,89] and we will accept the μOMT results as the accurate values. Because the SCT and μOMT transmission coefficients constants agree to three significant figures at all temperatures studied, it is clear that the small-curvature tunneling mechanism dominates even though a light atom is being transferred between two heavy atoms. The asymmetric Eckart model overestimates Γ by as much as a factor of 4. This might be due in part to an overestimate by BB1K/6-31+G(d,p) of the imaginary frequency ($\nu^* = 1666i\ \mathrm{cm}^{-1}$) used in the Eckart calculations. However, given the accuracy of BB1K for transition structure energies and geometries discussed above, the BB1K imaginary frequency should be reliable as well. The dominant source of error is likely the fact the Eckart potential is substantially narrower than the true $\Delta G^{GT,0}(T,s)$ curve at its base, as noted in previous studies.[90,91]

Finally, performing a standard three-parameter fit ($k = AT^n \exp(-E_a/RT)$) to the CUS/μOMT rate constants yields the expression $k = (9.35 \times 10^8)T^{0.994} \exp(-1.12 \times 10^4/T)\ \mathrm{s}^{-1}$. In Figure 4, we compare Arrhenius plots of the CUS/μOMT rate constant with the rate constants predicted from non-variational transition state theory (TST) and Marinov's estimated expression[21] of $k = (6.00 \times 10^{10}) \exp(-1.23 \times 10^4/T)\ \mathrm{s}^{-1}$. The discrepancy between the TST and CUS/μOMT rate constants is significant only at lower temperatures. The Marinov rate constants are approximately 2 orders of magnitude lower than the CUS/μOMT values at all temperatures plotted. At lower temperatures, this is due to the higher value of E_a in Marinov's equation. At higher temperatures, this is due to the lack of a temperature dependence in the pre-exponential factor of Marinov's equation. In any case, our calculations indicate that the 1,5-hydrogen shift in the β-hydroxyethylperoxy radical plays a more important role in the combustion of ethanol than previously believed. However, the room-temperature CUS/μOMT rate constant of $1.05 \times 10^{-5}\ \mathrm{s}^{-1}$ confirms that the thermal reaction is far too slow to play a role in atmospheric chemistry.

TABLE 10: Variational Transition State Theory Results for Reaction 1[a]

		rate constant (s^{-1})			transmission coefficient			
T(K)	s_*^{CVT}	TST	CVT	CUS	SCT	LCT	μOMT	Eckart
200	0.221	1.19×10^{-14}	5.84×10^{-15}	5.80×10^{-15}	13.51	7.00	13.51	58.37
250	0.216	1.97×10^{-9}	1.21×10^{-9}	1.20×10^{-9}	5.37	3.31	5.37	16.37
298	0.211	4.53×10^{-6}	3.23×10^{-6}	3.20×10^{-6}	3.29	2.28	3.29	7.99
400	0.198	1.33×10^{-1}	1.16×10^{-1}	1.14×10^{-1}	1.95	1.56	1.95	3.60
600	−0.009	3.13×10^{3}	3.13×10^{3}	3.10×10^{3}	1.35	1.21	1.35	2.00
800	−0.018	5.05×10^{5}	5.03×10^{5}	4.99×10^{5}	1.19	1.11	1.19	1.60
1000	−0.026	1.11×10^{7}	1.10×10^{7}	1.09×10^{7}	1.12	1.07	1.12	1.42
1200	−0.033	8.87×10^{7}	8.76×10^{7}	8.70×10^{7}	1.08	1.05	1.08	1.32
1400	−0.040	3.99×10^{8}	3.93×10^{8}	3.90×10^{8}	1.06	1.04	1.06	1.26
1600	−0.046	1.25×10^{9}	1.22×10^{9}	1.21×10^{9}	1.04	1.03	1.04	1.22
1800	−0.052	3.04×10^{9}	2.98×10^{9}	2.96×10^{9}	1.03	1.02	1.03	1.19
2000	−0.057	6.25×10^{9}	6.09×10^{9}	6.05×10^{9}	1.03	1.02	1.03	1.17

[a] Based on BB1K/6-31+G(d,p) energies, gradients, and Hessians.

TABLE 11: Variational Transition State Theory Results for Reaction 2[a]

	rate constant (s^{-1})		transmission coefficient			
T(K)	TST	CVT	SCT	LCT	μOMT	Eckart
200	7.81×10^{-11}	7.81×10^{-11}	5.42×10^{9}	1.96×10^{10}	1.97×10^{10}	1.98×10^{13}
250	3.59×10^{-6}	3.59×10^{-6}	5.85×10^{6}	1.06×10^{7}	1.11×10^{7}	1.46×10^{9}
298	3.60×10^{-3}	3.60×10^{-3}	1.01×10^{5}	1.18×10^{5}	1.38×10^{5}	4.30×10^{6}
400	3.46×10^{1}	3.46×10^{1}	7.83×10^{2}	5.40×10^{2}	8.44×10^{2}	3.92×10^{3}
600	2.62×10^{5}	2.62×10^{5}	1.79×10^{1}	1.11×10^{1}	1.81×10^{1}	2.46×10^{1}
800	2.34×10^{7}	2.34×10^{7}	4.74	3.51	4.74	5.51
1000	3.53×10^{8}	3.53×10^{8}	2.64	2.18	2.64	3.05
1200	2.20×10^{9}	2.20×10^{9}	1.94	1.70	1.94	2.27
1400	8.21×10^{9}	8.21×10^{9}	1.62	1.47	1.62	1.90
1600	2.23×10^{10}	2.23×10^{10}	1.44	1.35	1.44	1.69
1800	4.87×10^{10}	4.87×10^{10}	1.33	1.26	1.33	1.56
2000	9.15×10^{10}	9.15×10^{10}	1.26	1.21	1.26	1.47

[a] Based on BB1K/6-31+G(d,p) energies, gradients, and Hessians.

III.E. Transition State Theory Calculations on the 1,4-Hydrogen Shift in the β-Hydroxyethoxy Radical. Table 11 presents the thermal rate constants and transmission coefficients predicted for Reaction 2:

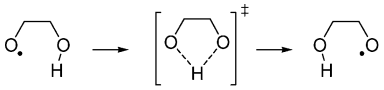

III **TS III** **III** [2]

There are a number of significant differences in the dynamics of Reactions 1 and 2. First, there is no variational effect on the rate constant for Reaction 2; at all temperatures studied, the transition state coincides exactly with the saddle point.

Second, tunneling has a far larger impact on the rate of Reaction 2. At 200 K, tunneling accelerates Reaction 2 by 9 orders of magnitude more than Reaction 1. Qualitatively, this is reasonable given the different curvatures of the minimum energy paths. As noted in Section III.D., the transition structure for Reaction 1 has an imaginary frequency of 1666i cm^{-1}. In contrast, the transition structure for Reaction 2 has an imaginary frequency of 3295i cm^{-1}, reflecting the existence of a far narrower adiabatic potential.

Third, unlike for Reaction 1, large-curvature tunneling plays an important role in the dynamics of Reaction 2. The LCT and μOMT transmission coefficients agree (to two significant figures) at 200 and 250 K, and small-curvature tunneling is not the dominant mechanism until the temperature reaches ~600 K. Such a change in tunneling mechanism with temperature was observed by Truhlar and co-workers[81] in their study of the reaction of CF_3 with CD_3H. At 298 and 400 K, the small-curvature and large-curvature mechanisms both contribute significantly to the overall tunneling. Corchado and co-workers[89] have noted that in such situations, even the μOMT method may underestimate the transmission coefficient.

The Eckart method again overestimates the extent of tunneling, especially at lower temperatures. At 200 K, the Eckart Γ value is 3 orders of magnitude higher than the μOMT Γ value. (Corchado and co-workers'[89] point notwithstanding, it is reasonable to assume that at 200 K the μOMT method provides a reliable estimate of tunneling.) This may call into question the use of the Eckart method in the study of other intramolecular hydrogen shift reactions, such as in the ethoxy system studied by Zhang et al.[25]

Finally, fitting the TST/μOMT rate constants for Reaction 2 yields the expression $k = (8.71 \times 10^{-10})T^{6.322} \exp(-2.54 \times 10^3/T)$ s^{-1}. In Figure 5, we compare Arrhenius plots of the TST/μOMT rate constant for Reaction 2 with the rate constants predicted for the same reaction from transition state theory without tunneling (TST). We also plot the Arrhenius expression derived by Vereecken and Peeters[1] ($k_\infty = (1.1 \times 10^{13}) \exp(-5.03 \times 10^3/T)$ s^{-1}) for the β-scission of **III** (Reaction 9):

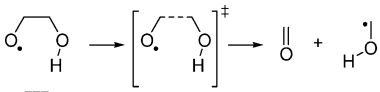

III [9]

First, we note the large curvature in the μOMT Arrhenius plot, showing the enormous impact of tunneling on the 1,4-hydrogen shift at lower temperatures. We also note that, even accounting for tunneling, the hydrogen shift reaction is 1−3 orders of magnitude slower than the β-scission reaction at all temperatures considered. The pre-exponential factor derived by Veerecken and Peeters for **III** is typical of β-scission reactions

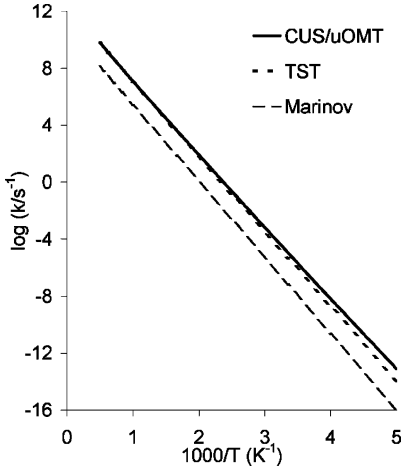

Figure 4. Arrhenius plots of the rate constants for Reaction 1 predicted by canonical unified statistical theory with microcanonical optimized multidimensional tunneling (CUS/μOMT), transition state theory (TST), and the approximate expression of Marinov.[21]

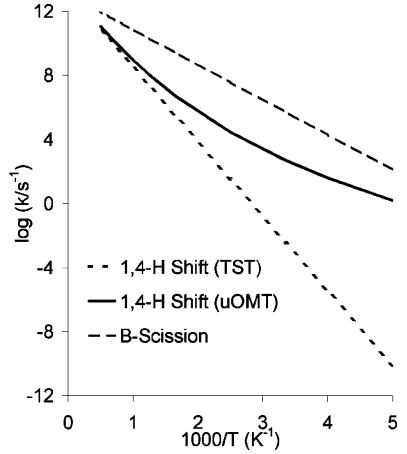

Figure 5. Arrhenius plots of the rate constants for the 1,4-hydrogen shift of species **III** (Reaction 2) predicted by transition state theory with microcanonical optimized multidimensional tunneling (μOMT) and by transition state theory (TST), and the rate constant for the β-scission of **III** determined by Vereecken and Peeters.[1]

for a wide variety of alkoxy radicals.[92] However, the β-scission activation energies for some alkoxy radicals are higher by at least a few kcals per mole.[92] This suggests that the 1,4-hydrogen shift could be competitive with β-scission in other alkoxy radicals found in the atmosphere.

IV. Conclusions

Our quantum chemical examination of the conformers and intramolecular hydrogen shift barriers for the β-hydroxyethylperoxy (**I**) and β-hydroxyethoxy (**III**) radicals lead to somewhat different conclusions from previous studies.[1,19] The B3LYP, MPW1K, and BB1K functionals all predict relative stabilities for the conformers of **I** and **III** in excellent agreement with the CBS-QB3 composite method if the basis set used in the DFT calculations includes diffuse functions on non-hydrogen atoms. Given the validation of CBS-QB3 against the G2 test set of thermochemical properties,[13] we are confident that the CBS-QB3 predictions are more accurate than the CCSD(T)/6-31G(d,p) calculations used in Vereecken and Peeters' study.[1]

However, for hydrogen abstraction reaction barriers, the MCG3 composite method is often more reliable than CBS-QB3.[33,54] The MCG3 barrier for the 1,5-hydrogen shift in **I** (Reaction 1) is 23.59 kcal/mol, and the average MCG3 barrier for the 1,4-hydrogen shift in **III** (Reaction 2) is 22.71 kcal/mol The MPW1K and BB1K methods predict barriers that are rather close to these predictions, while the B3LYP method, as well as composite methods based on B3LYP-optimized geometries, are on the whole significantly less accurate. Our inability to obtain valid QCISD and MC-QCISD geometries for the hydrogen shift transition structures is admittedly problematic and perhaps makes our results here less conclusive. Nevertheless, our calculations do suggest that Olivella and Solé's[19] RCCSD/6-311+G(3df,2p) barrier of 29.37 kcal/mol for Reaction 1 is too high.

Our RRKM/master equation simulations do, nevertheless, support Olivella and Solé's[19] contention that the 1,5-hydrogen shift in chemically activated **I** may play an important role in the troposphere. Our simulations also suggest that the 1,4-hydrogen shift may play a non-negligible role at low pressures, due in part to the fact that multiple conformers of **I** can undergo this reaction. The competition between the 1,5-hydrogen shift (and other prompt reactions) vs collisional stabilization is a sensitive function of the extent to which species **I** is chemical activated. B3LYP, MPW1K, and BB1K calculations all predict the existence of an enthalpic barrier for the formation of **I** from O_2 and $\bullet C_2H_4OH$, and therefore a greater degree of chemical activation than predicted by Olivella and Solé. Given that the addition of O_2 to alkyl radicals is typically barrierless, the $O_2 + \bullet C_2H_4OH$ potential energy surface should be examined at higher levels of theory to confirm or refute our DFT predictions.

Finally, our variational transition state theory calculations indicate that tunneling plays a rather modest role in the dynamics of Reaction 1, but a dramatic role in the dynamics of Reaction 2. However, even with such large transmission coefficients, the 1,4-hydrogen shift will usually be far slower than β-scission for alkoxy radicals. This will not be the case for 1,4-hydrogen shifts in closed-shell systems such as syn carbonyl oxides, and calculations of tunneling effects on the dynamics of such systems are currently underway.

For both reactions, the Eckart transmission coefficients are significantly larger than the accurate μOMT transmission coefficients. However, the cost of an Eckart calculation is trivial compared to a μOMT calculation, and Eckart transmission coefficients can be adequate if one needs to estimate tunneling effects for a large number of reactions. Nevertheless, when the thermal rate constant of a specific hydrogen shift reaction must be predicted accurately, there is no substitute for a rigorous multidimensional tunneling calculation.

Acknowledgment. This work was supported by the donors of the American Chemical Society Petroleum Research Fund (38037-GB6 and 44764-B6), the National Science Foundation (ATM0352926), and the Violet Olson Beltmann and the Student-Faculty Summer Research Collaboration Funds of Macalester College. Calculations were performed at Macalester College, SUNY-ESF, the National Computational Science Alliance facility at the University of Illinois (CHE070008), the University of Minnesota Supercomputing Institute, and the Midwest Undergraduate Computational Chemistry Consortium facility at Hope College (NSF-CHE0520704). We thank Dr. Benjamin Lynch (University of Minnesota) and Dr. Sudhakar Pamidighantam (University of Illinois) for generously providing technical advice. Finally, K.T.K. thanks Prof. Donald G. Truhlar for his hospitality and the freedom to wrestle with the ideas of transition state theory during a sabbatical visit, a freedom which ultimately led to the completion of this paper.

Supporting Information Available: Tables of selected geometrical parameters for the species in Reactions 1 and 2, discussion of these results, and figures presenting all of the species involved in the RRKM/master equation simulations. This material is available free of charge via the Internet at http://pubs.acs.org.

References and Notes

(1) Vereecken, L.; Peeters, J. *J. Phys. Chem. A* **1999**, *103*, 1768.
(2) Vereecken, L.; Peeters, J.; Orlando, J. J.; Tyndall, G. S.; Ferronato, C. *J. Phys. Chem. A* **1999**, *103*, 4693.
(3) Lei, W.; Zhang, R. *J. Phys. Chem. A* **2001**, *105*, 3808.
(4) Dibble, T. S. *J. Am. Chem. Soc.* **2001**, *123*, 4228.
(5) Dibble, T. S. *J. Phys. Chem. A* **1999**, *103*, 8559.
(6) Dibble, T. S. *Chem. Phys. Lett.* **1999**, *301*, 297.
(7) Dibble, T. S. *J. Phys. Chem. A* **2004**, *108*, 2199.
(8) Dibble, T. S. *J. Phys. Chem. A* **2004**, *108*, 2208.
(9) Stephens, P. J.; Devlin, F. J.; Chabalowski, C. F.; Frisch, M. J. *J. Phys. Chem.* **1994**, *98*, 11623.
(10) Becke, A. D. *J. Chem. Phys.* **1993**, *98*, 5648.
(11) Lee, C.; Yang, W.; Parr, R. G. *Phys. Rev. B* **1988**, *37*, 785.
(12) Lynch, B. J.; Fast, P. L.; Harris, M.; Truhlar, D. G. *J. Phys. Chem. A* **2000**, *104*, 4811.
(13) Montgomery, J. A., Jr.; Frisch, M. J.; Ochterski, J. W.; Petersson, G. A. *J. Chem. Phys.* **1999**, *110*, 2822.
(14) Eckart, C. *Phys. Rev.* **1930**, *35*, 1303.
(15) Sawada, S.; Totsuka, T. *Atmos. Environ.* **1986**, *20*, 821.
(16) Niki, H.; Maker, P. D.; Savage, C. M.; Breitenbach, L. P. *J. Phys. Chem.* **1978**, *82*, 135.
(17) Zador, J.; Wagner, V.; Wirtz, K.; Pilling, M. J. *Atmos. Environ.* **2005**, *39*, 2805.
(18) Niki, H.; Maker, P. D.; Savage, C. M.; Breitenbach, L. P. *Chem. Phys. Lett.* **1981**, *80*, 499.
(19) Olivella, S.; Solé, A. *J. Phys. Chem. A* **2004**, *108*, 11651.
(20) Boyd, A. A.; Lesclaux, R. *Int. J. Chem. Kinet.* **1997**, *29*, 323.
(21) Marinov, N. M. *Int. J. Chem. Kinet.* **1999**, *31*, 183.
(22) Westbrook, C. K.; Pitz, W. J.; Curran, H. J. *J. Phys. Chem. A* **2006**, *110*, 6912.
(23) Atkinson, R. *Int. J. Chem. Kinet.* **1997**, *29*, 99.
(24) Orlando, J. J.; Tyndall, G. S.; Bilde, M.; Ferronato, C.; Wallington, T. J.; Vereecken, L.; Peeters, J. *J. Phys. Chem. A* **1998**, *102*, 8116.
(25) Zhang, Y.; Zhang, S.; Li, Q. S. *Chem. Phys.* **2005**, *308*, 109.
(26) Senosiain, J. P.; Musgrave, C. B.; Golden, D. M. *J. Phys. Chem. A* **2001**, *105*, 1669.
(27) Truhlar, D. G.; Kuppermann, A. *J. Am. Chem. Soc.* **1971**, *93*, 1840.
(28) Kreevoy, M. M.; Ostovic, D.; Truhlar, D. G.; Garrett, B. C. *J. Phys. Chem.* **1986**, *90*, 3766.
(29) Zhang, J.-G.; Li, Q. S.; Zhang, S.-W. *J. Mol. Model.* **2006**, *2006*, 190.
(30) Scott, A. P.; Radom, L. *J. Phys. Chem.* **1996**, *100*, 16502.
(31) Lynch, B. J.; Truhlar, D. G. *J. Phys. Chem. A* **2001**, *105*, 2936.
(32) Zhao, Y.; Lynch, B. J.; Truhlar, D. G. *J. Phys. Chem. A* **2004**, *108*, 2715.
(33) Coote, M. L. *J. Phys. Chem. A* **2004**, *108*, 3865.
(34) Jursic, B. S. *J. Mol. Struct. (Theochem)* **1998**, *430*, 17.
(35) Kobayashi, Y.; Kamiya, M.; Hirao, K. *Chem. Phys. Lett.* **2000**, *319*, 695.
(36) Adamo, C.; Barone, V. *J. Chem. Phys.* **1998**, *108*, 664.
(37) Perdew, J. P.; Chevary, J. A.; Vosko, S. H.; Jackson, K. A.; Pederson, M. R.; Singh, D. J.; Fiolhais, C. *Phys. Rev. B* **1992**, *46*, 6671.
(38) Becke, A. D. *Phys. Rev. A* **1988**, *38*, 3098.
(39) Becke, A. D. *J. Chem. Phys.* **1996**, *104*, 1040.
(40) Hehre, W. J.; Ditchfield, R.; Pople, J. A. *J. Chem. Phys.* **1972**, *56*, 2257.
(41) Hariharan, P. C.; Pople, J. A. *Theoret. Chim. Acta.* **1973**, *28*, 213.
(42) Clark, T.; Chandrasekhar, J.; Spitznagel, G. W.; Schleyer, P. v. R. *J. Comput. Chem.* **1983**, *4*, 294.
(43) Lynch, B. J.; Zhao, Y.; Truhlar, D. G. *J. Phys. Chem. A* **2003**, *107*, 1384.
(44) Curtiss, L. A.; Redfern, P. C.; Raghavachari, K.; Rassolov, V.; Pople, J. A. *J. Chem. Phys.* **1999**, *110*, 4703.
(45) Curtiss, L. A.; Raghavachari, K.; Redfern, P. C.; Pople, J. A. *J. Chem. Phys.* **2000**, *112*, 1125.
(46) Baboul, A. G.; Curtiss, L. A.; Redfern, P. C.; Raghavachari, K. *J. Chem. Phys.* **1999**, *110*, 7650.
(47) Curtiss, L. A.; Redfern, P. C.; Raghavachari, K.; Pople, J. A. *J. Chem. Phys.* **2001**, *114*, 108.
(48) Lynch, B. J.; Truhlar, D. G. *J. Phys. Chem. A* **2003**, *107*, 8996.
(49) Mackie, J. C.; Bacskay, G. B. *J. Phys. Chem. A* **2005**, *109*, 11967.
(50) Dybala-Defratyka, A.; Paneth, P.; Pu, J.; Truhlar, D. G. *J. Phys. Chem. A* **2004**, *108*, 2475.
(51) Chuang, Y.-Y.; Coitino, E. L.; Truhlar, D. G. *J. Phys. Chem. A* **2000**, *104*, 446.
(52) Lynch, B. J.; Truhlar, D. G. *J. Phys. Chem. A* **2002**, *106*, 842.
(53) Fast, P. L.; Truhlar, D. G. *J. Phys. Chem. A* **2000**, *104*, 6111.
(54) Lynch, B. J.; Truhlar, D. G. *J. Phys. Chem. A* **2003**, *107*, 3898.
(55) Frisch, M. J.; Trucks, G. W.; Schlegel, H. B.; Scuseria, G. E.; Robb, M. A.; Cheeseman, J. R.; Montgomery, J. A., Jr.; Vreven, T.; Kudin, K. N.; Burant, J. C.; Millam, J. M.; Iyengar, S. S.; Tomasi, J.; Barone, V.; Mennucci, B.; Cossi, M.; Scalmani, G.; Rega, N.; Petersson, G. A.; Nakatsuji, H.; Hada, M.; Ehara, M.; Toyota, K.; Fukuda, R.; Hasegawa, J.; Ishida, M.; Nakajima, T.; Honda, Y.; Kitao, O.; Nakai, H.; Klene, M.; Li, X.; Knox, J. E.; Hratchian, H. P.; Cross, J. B.; Bakken, V.; Adamo, C.; Jaramillo, J.; Gomperts, R.; Stratmann, R. E.; Yazyev, O.; Austin, A. J.; Cammi, R.; Pomelli, C.; Ochterski, J. W.; Ayala, P. Y.; Morokuma, K.; Voth, G. A.; Salvador, P.; Dannenberg, J. J.; Zakrzewski, V. G.; Dapprich, S.; Daniels, A. D.; Strain, M. C.; Farkas, O.; Malick, D. K.; Rabuck, A. D.; Raghavachari, K.; Foresman, J. B.; Ortiz, J. V.; Cui, Q.; Baboul, A. G.; Clifford, S.; Cioslowski, J.; Stefanov, B. B.; Liu, G.; Liashenko, A.; Piskorz, P.; Komaromi, I.; Martin, R. L.; Fox, D. J.; Keith, T.; Al-Laham, M. A.; Peng, C. Y.; Nanayakkara, A.; Challacombe, M.; Gill, P. M. W.; Johnson, B.; Chen, W.; Wong, M. W.; Gonzalez, C.; Pople, J. A. *Gaussian 03*, revision B.05; Gaussian Inc.: Pittsburgh, PA, 2003.
(56) Stanton, J. F.; Gauss, J.; Watts, J. D.; Szalay, P. G.; Bartlett, R. J.; Auer, A. A.; Bernholdt, D. B.; Christiansen, O.; Harding, M. E.; Heckert, M.; Heun, O.; Huber, C.; Jonsson, D.; Jusélius, J.; Lauderdale, W. J.; Metzroth, T.; Michauk, C.; Price, D. R.; Ruud, K.; Schiffmann, F.; Tajti, A.; Varner, M. E.; Vázquez, J. *ACES2*, Mainz-Austin-Budapest Version; 2005.
(57) Zhao, Y.; Rodgers, J. M.; Lynch, B. J.; Fast, P. L.; Pu, J.; Chuang, Y.-Y.; Truhlar, D. G. *MULTILEVEL*, Version 4.0; Department of Chemistry and Supercomputer Institute, University of Minnesota: Minneapolis, MN, 2004.
(58) Barker, J. R.; Ortiz, N. F.; Preses, J. M.; Lohr, L. L.; Maranzana, A.; Stimac, P. J. *MultiWell 2.02*; University of Michigan: Ann Arbor, MI, 2006.
(59) Barker, J. R. *Int. J. Chem. Kinet.* **2001**, *33*, 232.
(60) Robinson, P. J.; Holbrook, K. A. *Unimolecular Reactions*; Wiley-Interscience: London, 1972.
(61) Barker, J. R.; Yoder, L. M.; King, K. D. *J. Phys. Chem. A* **2001**, *105*, 796.
(62) Mourits, F. M.; Rummens, F. H. A. *Can. J. Chem.* **1977**, *55*, 3007.
(63) Hippler, H.; Troe, J.; Wendelken, H. J. *J. Chem. Phys.* **1983**, *78*, 6709.
(64) McCann, D. W.; Danner, R. P. *Ind. Eng. Chem. Process Des. Dev.* **1984**, *23*, 529.
(65) Joback, K. G.; Reid, R. C. *Chem. Eng. Comm.* **1987**, *57*, 233.
(66) Reid, R. C.; Prausnitz, J. M.; Poling, B. E. *The Properties of Gases and Liquids*; McGraw-Hill: New York, 1987.
(67) Hirschfelder, J. O.; Curtiss, C. F.; Bird, R. B. *Molecular Theory of Gases and Liquids*; Wiley: New York, 1954.
(68) Kuwata, K. T.; Valin, L. C.; Converse, A. D. *J. Phys. Chem. A* **2005**, *109*, 10710.
(69) Snider, N. *J. Chem. Phys.* **1984**, *80*, 1885.
(70) Corchado, J. C.; Chuang, Y.-Y.; Fast, P. L.; Villà, J.; Hu, W.-P.; Liu, Y.-P.; Lynch, G. C.; Nguyen, K. A.; Jackels, C. F.; Melissas, V. S.; Lynch, B. J.; Rossi, I.; Coitino, E. L.; Ramos, A. F.; Pu, J.; Albu, T. V.; Steckler, R.; Garrett, B. C.; Isaacson, A. D.; Truhlar, D. G. *POLYRATE 9.1*; Department of Chemistry and Supercomputer Institute, University of Minnesota: Minneapolis, MN, 2003.
(71) Corchado, J. C.; Chuang, Y.-Y.; Coitiño, E. L.; Truhlar, D. G. *GAUSSRATE 9.1*; Department of Chemistry and Supercomputer Institute, University of Minnesota: Minneapolis, MN, 2003.
(72) Truhlar, D. G.; Garrett, B. C. *Acc. Chem. Res.* **1980**, *13*, 440.
(73) Truhlar, D. G.; Garrett, B. C.; Klippenstein, S. J. *J. Phys. Chem.* **1996**, *100*, 12771.
(74) Truhlar, D. G.; Hase, W. L.; Hynes, J. T. *J. Phys. Chem.* **1983**, *87*, 2664.
(75) Garrett, B. C.; Truhlar, D. G. *J. Phys. Chem.* **1980**, *84*, 805.
(76) Garrett, B. C.; Truhlar, D. G.; Grev, R. S.; Magnuson, A. W. *J. Phys. Chem.* **1980**, *84*, 1730.
(77) Garrett, B. C.; Truhlar, D. G. *J. Chem. Phys.* **1982**, *76*, 1853.
(78) Truhlar, D. G.; Gordon, M. S. *Science* **1990**, *249*, 491.
(79) Liu, Y.-P.; Lynch, G. C.; Truong, T. N.; Lu, D.-h.; Truhlar, D. G.; Garrett, B. C. *J. Am. Chem. Soc.* **1993**, *115*, 2408.
(80) Fernandez-Ramos, A.; Truhlar, D. G. *J. Chem. Phys.* **2001**, *114*, 1491.
(81) Liu, Y.-P.; Lu, D.-h.; González-Lafont, A.; Truhlar, D. G.; Garrett, B. C. *J. Am. Chem. Soc.* **1993**, *115*, 7806.
(82) Johnston, H. S. *Gas Phase Reaction Rate Theory*; Ronald Press: New York, 1966.

(83) Zhang, S.; Truong, T. N. *VKLab*, version 1.0; University of Utah: Salt Lake City, UT, 2001.
(84) Kuwata, K. T.; Templeton, K. L.; Hasson, A. S. *J. Phys. Chem. A* **2003**, *107*, 11525.
(85) Vereecken, L.; Peeters, J. *J. Chem. Phys.* **2003**, *119*, 5159.
(86) Corchado, J. C.; Truhlar, D. G.; Espinosa-Garcia, J. *J. Chem. Phys.* **2000**, *112*, 9375.
(87) Rangel, C.; Navarrete, M.; Corchado, J. C.; Espinosa-Garcia, J. *J. Chem. Phys.* **2006**, *124*, 1243061.
(88) Pu, J.; Truhlar, D. G. *J. Chem. Phys.* **2002**, *117*, 1479.
(89) Sanson, J. A.; Sanchez, M. L.; Corchado, J. C. *J. Phys. Chem. A* **2006**, *110*, 589.
(90) Isaacson, A. D.; Wang, L.; Scheiner, S. *J. Phys. Chem.* **1993**, *97*, 1765.
(91) Truong, T. N.; Duncan, W. T.; Tirtowidjojo, M. *Phys. Chem. Chem. Phys.* **1999**, *1*, 1061.
(92) Johnson, D.; Cassanelli, P.; Cox, R. A. *Atmos. Environ.* **2004**, *38*, 1755.